J. Fluid Mech. (1979), *vol.* 94, *part* 1, *pp.* 103–128
Printed in Great Britain

Dynamical instabilities and the transition to chaotic Taylor vortex flow

By P. R. FENSTERMACHER, HARRY L. SWINNEY†
Physics Department, City College of CUNY, New York, N.Y. 10031
AND J. P. GOLLUB
Physics Department, Haverford College, Haverford, PA 19041

(Received 5 July 1978 and in revised form 13 September 1978)

We have used the technique of laser-Doppler velocimetry to study the transition to turbulence in a fluid contained between concentric cylinders with the inner cylinder rotating. The experiment was designed to test recent proposals for the number and types of dynamical regimes exhibited by a flow before it becomes turbulent. For different Reynolds numbers the radial component of the local velocity was recorded as a function of time in a computer, and the records were then Fourier-transformed to obtain velocity power spectra. The first two instabilities in the flow, to time-independent Taylor vortex flow and then to time-dependent wavy vortex flow, are well known, but the present experiment provides the first quantitative information on the subsequent regimes that precede turbulent flow. Beyond the onset of wavy vortex flow the velocity spectra contain a single sharp frequency component and its harmonics; the flow is strictly periodic. As the Reynolds number is increased, a previously unobserved second sharp frequency component appears at $R/R_c = 10{\cdot}1$, where R_c is the critical Reynolds number for the Taylor instability. The two frequencies appear to be irrationally related; hence this is a quasi-periodic flow. A chaotic element appears in the flow at $R/R_c \simeq 12$, where a weak broadband component is observed in addition to the sharp components; this flow can be described as weakly turbulent. As R is increased further, the component that appeared at $R/R_c = 10{\cdot}1$ disappears at $R/R_c = 19{\cdot}3$, and the remaining sharp component disappears at $R/R_c = 21{\cdot}9$, leaving a spectrum with only the broad component and a background continuum. The observance of only two discrete frequencies and then chaotic flow is contrary to Landau's picture of an infinite sequence of instabilities, each adding a new frequency to the motion. However, recent studies of nonlinear models with a few degrees of freedom show a behaviour similar in most respects to that observed.

1. Introduction

Turbulent flows are the rule rather than the exception in nature, but our understanding of fluid flows is predominately of the laminar case. In turbulence theory most of the attention has been given to the fully developed case and relatively little to its onset. The theories of fully developed turbulence introduce a statistical description

† Present address: Department of Physics, The University of Texas at Austin, Austin, Texas 78712.

0022-1120/79/4318-7200 $02.00

ad hoc, an approach which assumes that a very large number of modes of the fluid are excited. However, the present study of the transition to turbulence indicates that the number of modes involved in the appearance of turbulence need not be large.

The flow between concentric rotating cylinders is a natural choice as a system for study because its high symmetry has made the study of the laminar regimes highly successful compared to more general flows. Although, as we shall see in what follows, a great deal remains unknown in this system, it is unlikely that a deeper understanding of the transition problem will come first from a more complex flow. Similarly, in the hope of obtaining deeper insight by restricting the problem we have chosen the case of the outer cylinder at rest with the inner cylinder rotating. The main reason for this choice is the apparent difference in the character of the transition to turbulence in this case as compared to the case where motion of the outer cylinder predominates. In the latter case, turbulence appears directly and catastrophically (Coles 1965). The hope is that a detailed study of a flow which is known to exhibit a sequence of instabilities will lead to insight into the onset of turbulence.

In § 2 we review briefly previous work on flow between concentric cylinders. Our fluid flow apparatus and laser-Doppler velocimetry system are described in § 3, and the experimental results are presented in § 4. These results are compared with other experiments in § 5 and with theory in § 6.

2. Review

The Reynolds number for the flow between concentric cylinders with the outer cylinder at rest can be defined as $R = r_i \Omega(r_o - r_i)/\nu$, where r_i and r_o are respectively the radii of the inner and outer cylinders, Ω is the angular velocity of the inner cylinder, and ν is the kinematic viscosity. Theoretical analyses for this system almost always assume the cylinders to be of infinite length, and most experiments have been done in long cylinders in an attempt to fulfil this assumption. We consider first the infinite cylinder results and then return at the end of this section to the question of the effect of finite cylinder length on the transition Reynolds numbers and the uniqueness of the flow.

2.1. *Time-independent flow*

At small Reynolds number the globally stable unique solution to the Navier–Stokes equations is $V_r = V_z = 0$, $V_\theta = Ar + B/r$, where r, θ, and z are cylindrical co-ordinates, and A and B are constants. Early research (Mallock 1888, 1896; Couette 1890) indicated that this flow becomes unstable as the Reynolds number is increased, but the nature of the instability was not established. In a classic study of hydrodynamic stability G. I. Taylor (1923) observed and explained the transition from azimuthal flow to a flow with horizontal toroidal vortices superimposed on the azimuthal flow, as shown in figure 1(*a*) (plate 1). Whereas Rayleigh's (1920) analysis showed that the azimuthal flow of an *inviscid* fluid is unstable at infinitesimally small Reynolds number, Taylor's linear stability analysis of the viscous fluid showed that viscosity delays the onset of the secondary flow to finite Reynolds number.

Taylor calculated the critical Reynolds number R_c and wavelength λ_c for the instability in the azimuthal flow for the narrow gap limit, $(r_o - r_i) \ll r_i$; the wide gap case was subsequently considered by Davey (1962), Walowit, Tsao & DiPrima (1964),

Roberts (1965), and others. Near R_c the equilibrium amplitude of the deviation from the azimuthal flow increases as $(R-R_c)^{\frac{1}{2}}$, as predicted by Landau (1944; Landau & Lifshitz 1959) and observed by Donnelly (1963). As R is increased further the flow develops significant spatial harmonic content in the axial direction. Davey (1962) expanded the velocity field in a spatial Fourier series in the axial direction and calculated the Reynolds number dependence of the Fourier coefficients, and his predictions were tested in experiments by Donnelly & Schwarz (1965), Snyder & Lambert (1966) and Gollub & Freilich (1976). Above R_c Burkhalter & Koschmieder (1973) found the axial wavelength remained constant if R was increased slowly, but experiments with different initial conditions produced stable stationary flows with wavelengths both greater and smaller than λ_c.

2.2. *Onset of time-dependent flow*

A number of workers from Taylor onward noted that with increasing Reynolds number there is a transition from time-independent Taylor vortex flow to a time-dependent flow. Schultz-Grunow & Hein (1956) obtained photographs of this time-dependent flow, which consists of transverse travelling waves superimposed on the horizontal vortices, as shown in figure 1 (*b*). A linear stability analysis of Taylor vortex flow analogous to that carried out by Taylor for the azimuthal flow is not possible because there is no simple closed solution for Taylor vortex flow. Davey, DiPrima & Stuart (1968) carried out a nonlinear analysis of the growth of Taylor vortices and examined their stability against small perturbations periodic in both z and θ; their analysis is applicable near the Taylor instability where the flow is not greatly different from the azimuthal flow. Retaining terms to the third order in the amplitude perturbation, they found that the time-independent vortex flow for the small gap limit becomes unstable at $R/R_c \simeq 1{\cdot}04$, which is sufficiently close to R_c so their approximations should be valid. A new flow is established which has waves travelling in the azimuthal direction. The mode with one wave around the annulus is the first to become unstable, but the two and four wave modes become unstable at only slightly higher Reynolds number. The validity of the neglect of terms higher than third order was supported by a subsequent calculation (Eagles 1971) to fifth order in the amplitude perturbation.

Other flow visualization studies of the onset of wavy vortex flow have been reported by Schwarz, Springett & Donnelly (1964), Coles (1965), Snyder (1968*a*, 1970) and Cole (1976). Eagles (1974) has calculated the torque necessary to maintain wavy vortex flow, and the results agreed well with measurements by Donnelly (1958) and Donnelly & Simon (1960). Meyer (1969) calculated numerically the wave velocity at three Reynolds numbers near the onset of wavy vortex flow and he obtained agreement with the measurements of Coles (1965).

2.3. *Transition to turbulence*

We have cited only a few references from the extensive literature that has developed on Taylor vortex flow, but we have mentioned all major references of which we are aware from the small body of literature on the onset of wavy vortex flow. (It should be mentioned again that our comments apply to the case when the outer cylinder is at rest.) The literature describing the flow for larger Reynolds numbers is quite sparse:

several papers mention that beyond the onset of the wavy flow there is a gradual transition to turbulence, but the only systematic detailed study of this transition was by Coles (1965). Coles' photographs of the flow showed that as the Reynolds number increased the fluid appears increasingly noisy, as shown in figure 1(*c*), and at sufficiently large Reynolds number the azimuthal waves disappear while the vortex structure remains, as shown in figure 1(*d*). (The disappearance of the waves was also observed by Schultz-Grunow & Hein (1956); Burkhalter & Koschmieder (1973); Koschmieder (1975).) Coles used a photocell to measure the frequency of the travelling waves passing an observation point, and he found that as R was increased beyond the onset of wavy flow the wave frequency decreased from $0{\cdot}5\Omega$ to $0{\cdot}34\Omega$, and for larger R the frequency was constant until the waves became lost in the noise. Coles concluded that 'at sufficiently large Reynolds numbers the discrete spectrum changes gradually and reversibly to a continuous one by broadening of the initially sharp spectral lines'; however, this conclusion was reached from inspection of the flow photographs and not from spectra.

2.4. *Effect of finite annulus height*

Cole (1976) has investigated the effect of finite annulus height on the transitions to Taylor vortex flow and wavy vortex flow. Although the analytic theory has been developed only for the infinite cylinder problem, Taylor vortex flow has been observed in experiments with annuli so short that only a few vortices can develop. In short annuli vortices appear at the ends of the annulus at Reynolds numbers well below the critical number for Taylor vortex flow in an infinite cylinder (Coles 1965; Cole 1976; Benjamin 1978). As the Reynolds number is increased the vortex pattern spreads toward the centre of the annulus, filling it at a Reynolds number that is within the experimental uncertainty equal to the critical Reynolds number for the infinite cylinder problem (Snyder 1968*b*; Cole, 1976). However, since the transition is entirely continuous, there is actually 'no bifurcation with which a particular value of R can be associated unambiguously, so experimental estimates are necessarily subjective to some extent...' (Benjamin 1978).

Cole (1976) found that the Reynolds number for onset of wavy vortex flow increases considerably as the annulus height is reduced. The theoretical prediction for the infinite cylinder was reached within a per cent or so only for annulus height to gap ratios of the order of 100 or greater. The height to gap ratio in the system studied by D. Coles (1965) was 27·9 and, in the present study, 20·0, and these annuli both have inner to outer cylinder radius ratios of $\frac{7}{8}$. J. A. Cole's study (1976) shows that for these annuli the transition to wavy vortex flow occurs at Reynolds numbers approximately 9 % and 13 %, respectively, greater than the theoretical value for an infinite cylinder.

2.5. *Uniqueness*

At sufficiently small Reynolds numbers there is for any flow geometry a unique stable solution to the Navier–Stokes equations; regardless of the initial conditions the flow will asymptotically approach this solution (Serrin 1959). However, at larger Reynolds numbers there can be multiple stable solutions to the equations of motion. The possibility of nonunique stable flows was not appreciated until the work of Coles (1965), but was vividly demonstrated by his surprising discovery that in the flow in his

concentric cylinder system as many as 26 distinct stable spatial states could be achieved at a given Reynolds number. The states were distinguished by the number of axial vortices p, which ranged from 18 to 32, and the number of azimuthal waves m, which ranged from 3 to 7. Different states p/m were produced by approaching the final Reynolds number with different acceleration rates and by rotating and then stopping the outer cylinder. Snyder (1969*a*, *b*) subsequently found that different axial states were also accessible in the time-independent Taylor vortex flow regime, and Burkhalter & Koschmieder (1974) found that the range of axial wavelengths for stable stationary states is quite large. Benjamin (1978) has observed distinct spatial states in Taylor vortex flow even in an annulus so short that only three or four vortices could be accommodated. The non-uniqueness and the associated hysteresis in the transitions between different spatial states greatly complicates investigations of the flow beyond the primary instability. Coles (1965, p. 416) wrote 'The central experimental difficulty is that an observer who knows the current steady operating conditions for the apparatus (geometry, fluid properties, speed), but does not know the previous operating history, will be unable to specify the two characteristic wavenumbers which are needed to determine the flow in detail'.

The vexing related problems of non-uniqueness and the effect of finite annulus height are formidable and are well beyond the present techniques of nonlinear hydrodynamic stability theory (DiPrima & Eagles 1977). Recently, Benjamin (1978) has applied concepts from catastrophe theory to explain the softening of the transition to Taylor vortex flow in a finite height annulus. Clearly additional theoretical research is necessary to understand how distinct stable spatial states develop and to understand the transitions between these states. In the present study, however, it is shown that, although the uniqueness problem is not understood, insight into the transition to turbulence can be gained by exploring the dynamical regimes exhibited by a single spatial state (see §§ 3.5 and 4.2).

3. Experimental techniques

3.1. *Concentric cylinder flow system*

Values for the apparatus parameters are given in table 1. The flow is parametrized by the Reynolds number, the ratio of cylinder radii, and the ratio of the fluid height to the gap between the cylinders. Thus precise control and measurement of these variables is essential.

A uniform and stable rate of rotation of the inner cylinder is obtained by the use of a synchronous motor driven by the output of a precision oscillator. The cylinder is mounted on a vibration-isolation table and is driven by a belt from a motor which is mounted away from the table. The motor frequency is quite stable, but the rotation period of the belt-driven cylinder, which is measured with an electronic timer, fluctuates by about 0·04 % (r.m.s.) in ten cycles due to the flexibility of the belt.

The cylindrical cell system is contained inside a large box which is maintained at a uniform temperature by forced air circulation. Since the viscosity of the sample fluid (water) varies by approximately 2 %/°C, the temperature must be precisely controlled and measured in order to have a well-defined Reynolds number. A temperature stability of $\pm 0{\cdot}05$ °C was achieved with a proportional controller which drives a heating element inside the box; the 0·05 °C temperature variation corresponds to a

Inner cylinder radius r_i	$2{\cdot}224 \pm 0{\cdot}001$ cm
Outer cylinder radius r_o	$2{\cdot}536 \pm 0{\cdot}005$ cm
Ratio of radii r_i/r_o	0·877
Horizontal fluid surfaces: upper	free
lower	rigid
Fluid height h	$6{\cdot}25 \pm 0{\cdot}02$ cm
Height/gap: $h/(r_o-r_i)$	20·0
Fluid kinematic viscosity (water):† 27·50 °C	$8{\cdot}45 \times 10^{-3}$ cm^2 s^{-1}
30·00 °C	$8{\cdot}01 \times 10^{-3}$ cm^2 s^{-1}
60·00 °C	$4{\cdot}95 \times 10^{-3}$ cm^2 s^{-1}
Number of axial vortices	17‡
Axial wavelength λ relative to the gap (at mid-height of the cylinder), $\lambda/(r_o-r_i)$	2·36
Number of waves around annulus in wavy state	4
Diameter of light scattering particles (less than 0·03 vol. %)	0·48 μm§
Sample dimensions for the velocity measurements (length × diameter)	0·13 × 0·03 mm
Critical Reynolds no., R_c (calculated from table 3A in Roberts, 1965)	119·1

† From the *Handbook of Chemistry and Physics*, 56th ed. (CRC, Cleveland, 1975).
‡ Measurements were also made with 15 vortices.
§ Measurements were also made with 0·365 μm diameter particles.

TABLE 1. Concentric cylinder fluid flow system with the inner cylinder rotating and the outer cylinder at rest.

viscosity variation of 0·1 %. The Reynolds number can be varied by changing the rotation frequency of the inner cylinder or the viscosity. Most measurements were made at 27·5 °C, but to determine the effect of varying the viscosity some measurements were also made at 30 °C and 60 °C (see table 1 and figure 5*g*). No significant difference was observed in the velocity power spectra obtained at the same Reynolds number with different rotation frequencies and viscosities.

The scattering particles for the laser-Doppler measurements were polystyrene spheres, either 0·480 or 0·365 μm in diameter. The concentration by volume was 0·03 %, which changes the viscosity by only 0·05 %.

3.2. *Photographic studies and wavelength determination*

The flow pattern was visualized by seeding the flow with Kalliroscope AQ1000 suspension.† Fluid flow pictures were taken on 10·2 × 12·7 cm Kodak Tri-X Pan professional film with a small aperture to provide depth of field. A measured exposure time of 50 μs, provided by dual electronic flashes, freezes the motion to within one-half the resolving power of the film. The prints were made on Kodak F-4 AZO paper developed in normal Kodak Dektol for 1·5 minutes. The same flow cell, temperature control and motor drive were used for both photographic and laser-Doppler measurements.

The positions of the vortex boundaries were measured with a cathetometer over a wide range of Reynolds number for several of the spatial states with different numbers of axial vortices and azimuthal waves. The number of azimuthal waves was determined either from Polaroid photographs or from measurements of the vortex wave frequency made with a small helium–neon laser and a photocell. The graphs of the vortex boundary positions were extremely useful in determining the spatial state in the

† Kalliroscope Corporation, Cambridge, Massachusetts 02142.

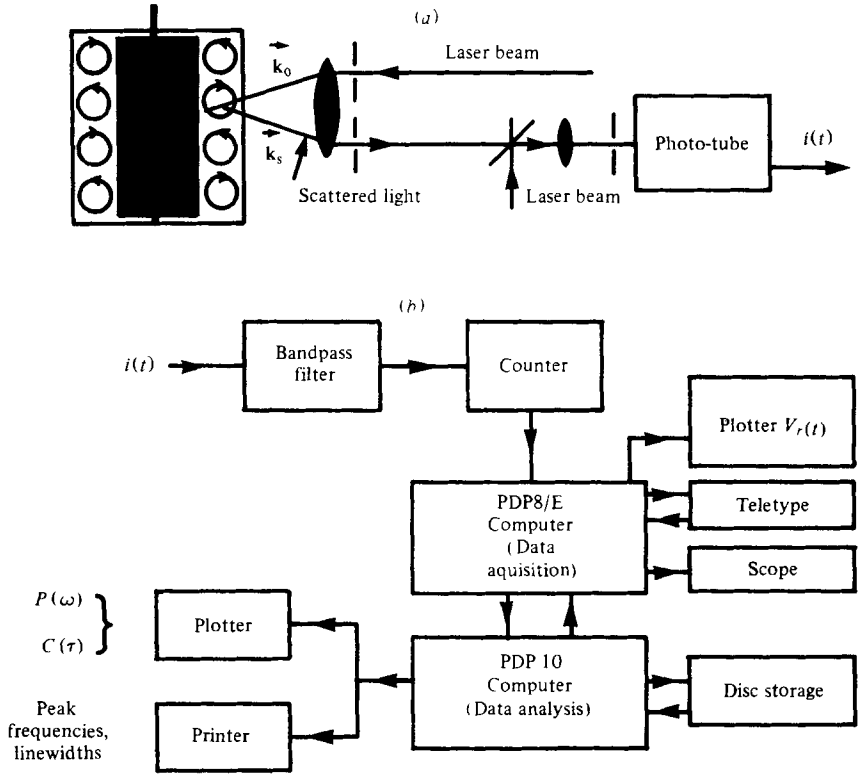

FIGURE 2. Schematic diagram of laser-Doppler velocimetry system. (*a*) Optical system. (*b*) Digital data acquisition and analysis electronics.

laser-Doppler measurements. The flow visualization measurements of the vortex boundaries and the laser-Doppler measurements of the velocity extrema agreed within 0·3 mm, which is 4 % of an axial wavelength. The ability to determine easily the spatial state was essential for our laser-Doppler study since the characteristic frequencies and transition Reynolds numbers are different for different spatial states.

3.3. *Laser-Doppler velocimetry optical system*

The optical part of the laser-Doppler system, which uses the reference beam backscatter geometry, is shown schematically in figure 2(*a*). (The laser-Doppler technique is discussed by Durrani & Greated (1977).) In our system the laser beam is spatially filtered and collimated and then focused onto the fluid with a 5·5 cm focal length lens. The laser power incident on the fluid is 100 mW or less. The light backscattered at a 155° angle is collected by the same lens and passes through a pinhole aperture which limits the collection angle to approximately one coherence solid angle. The scattered light then passes through a beamsplitter and is focused together with a reference beam from the laser onto a photomultiplier tube. The scattering volume in the fluid is approximately a prolate ellipsoid of revolution, with a major diameter of 0·13 mm (in the radial direction) and a minor diameter of 0·03 mm; thus the linear dimension of

the scattering volume in the radial direction is approximately one-twentieth of the gap between the cylinders.

The incident wavevector $\mathbf{k}_0$ and the scattered wavevector $\mathbf{k}_s$ are both in a vertical plane which passes through the cylinder axis. These wavevectors are at equal angles with respect to the horizontal plane so the momentum transfer vector $\mathbf{q} = \mathbf{k}_0 - \mathbf{k}_s$ is in the horizontal plane; hence the scattered light is Doppler-shifted in frequency by

$$\omega_D = \mathbf{V}.\mathbf{q} = V_r q = [(4\pi n/\lambda_0)\sin\tfrac{1}{2}\theta]\, V_r,$$

where n is the refractive index (1·333), λ_0 is the laser wavelength (488·0 nm), θ is the scattering angle (155°), and $V_r(\mathbf{r}, t)$ is the radial component of the fluid velocity. The Doppler-shifted scattered optical field is mixed with unshifted laser light at the photocathode, and the photocurrent $i(t)$, being proportional to the square of the incident field, oscillates at the Doppler shift frequency.

3.4. *Data acquisition system and spectral analysis*

The data acquisition and analysis system is diagrammed in figure 2(*b*). The photocurrent is amplified and bandpass filtered, and then clipped and counted for a fixed time interval Δt. At the end of each counting interval Δt the count is transferred to the memory of a Digital Equipment Corporation PDP 8/E minicomputer. In this way the frequency of the Doppler signal (and thus the fluid velocity) is simultaneously measured, digitized, and stored as a time history in sequential locations of computer memory. The measured Doppler shifts are typically 10^5 Hz, while the characteristic frequencies of the velocity field range from $\sim$ 0·1 to 10 Hz; hence the Doppler shifts, determined in a time short compared to the characteristic time for the velocity field to change, yield essentially the instantaneous velocity. In a strongly turbulent flow where the characteristic frequencies can be comparable to the Doppler shift a more sophisticated measurement scheme is generally necessary.

The data are transferred from the minicomputer to a Digital Equipment Corporation PDP-10 computer for analysis. The power spectral density of the velocity is obtained from the squared modulus of the fast Fourier transform of the digital velocity record. The velocity *vs.* time record, the velocity power spectrum, and velocity autocorrelation function are graphed on a digital plotter, and another program computes and lists the frequencies (first frequency moment) and linewidths (second frequency moment) of all spectral lines.

The GEO window (Otnes & Enochson 1978) is applied to each spectrum to suppress side lobes in the raw Fourier transform. If no averaging is employed to reduce statistical noise, the frequency resolution (defined as the full-width at half-maximum of a spectral line) is approximately $2/T$, where T is the length of the data record. The maximum frequency in a spectrum is the Nyquist frequency, $\omega_N = (2\Delta t)^{-1}$. Since both high resolution and a broad spectral range are needed to distinguish between different dynamical regimes in a flow, data records should contain as many samples ($n = T/\Delta t$) as possible. Our early experiments (Gollub & Swinney 1975) had velocity records with 1024 points, while the records in the present experiment have 8192 points. Moreover, the resolution has been improved by a factor of 40 rather than a factor of 8 by using longer sample intervals in the highest resolution spectra. The marked improvement in

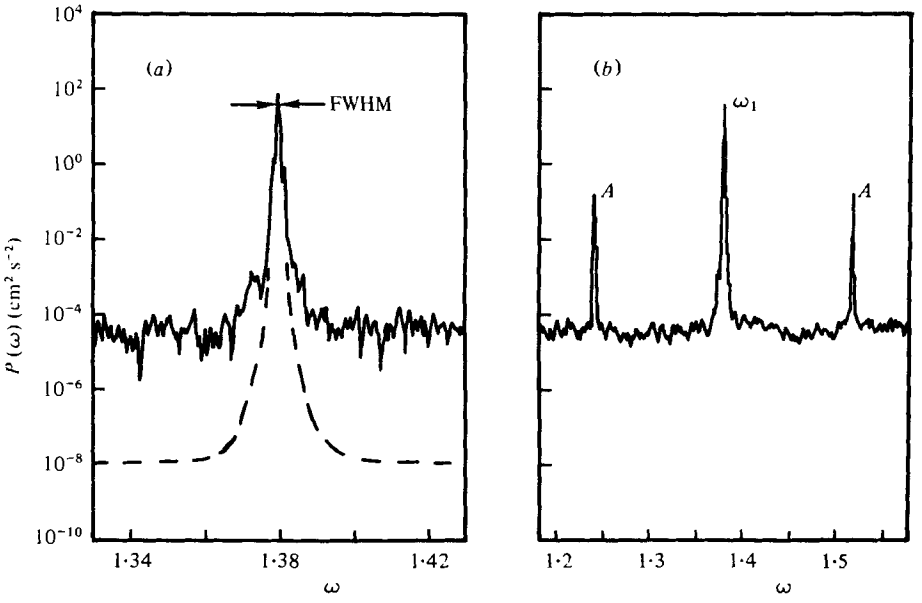

FIGURE 3. Segments of a velocity power spectrum computed from a velocity record obtained at $R/R_c = 5{\cdot}7$. The dimensionless frequency ω is in units of the cylinder frequency and the full spectrum extends from $\omega = 0$ to 2. (*a*) The solid curve is a high resolution plot with no smoothing; the spectral line is the fundamental frequency component corresponding to the azimuthal waves. The spectrum for a pure sine wave with the same centre frequency is shown by the dashed curve (see text). The lineshape and linewidth [full-width at half-maximum (FWHM)] of the fluid spectral component is the same as that of the pure sine wave. (*b*) The spectral component ω_1 at $\omega = 1{\cdot}380$ has harmonics $2\omega_1$, $3\omega_1$, etc. which lie beyond the spectral range sampled, $\omega = 0$ to 2. These higher frequency components appear as 'aliases' folded into the $\omega = 0$ to 2 spectrum. For example, the component A on the left is at $2\omega_N - 2\omega_1 = 1{\cdot}240$, where $\omega_N = 2{\cdot}000$ is the Nyquist frequency; the component A on the right is at $4\omega_1 - 2\omega_N = 1{\cdot}520$.

resolution has clarified considerably the transition picture [e.g., cf. figure 1 of Gollub and Swinney (1975) with figure 5 of the present paper].

The theoretical resolution (full-width at half-maximum of a spectral line) of an unsmoothed power spectrum of an 8192 point record processed with the GEO window is 0·04 % of the Nyquist frequency (Otnes & Enochson, 1978). This theoretical estimate of the resolution has been verified for our system by using the full 36 bit accuracy of the PDP-10 computer to compute the power spectrum of a pure sine wave with values synthesized as 12 bit integers (to simulate the 12 bit numbers in the PDP-8) for 8192 values of the argument. The spectrum of the pure sine wave record is shown on a plot with an expanded frequency scale in figure 3(*a*) along with the fluid spectral component corresponding to the azimuthal waves.

Figure 3(*a*) illustrates two general observations: (1) In our spectra the digitizing noise is at least three orders of magnitude smaller than other noise sources. (2) Even in the highest resolution spectra, the linewidth of the sharp spectral lines is determined solely by the instrumental resolution, i.e. by the length of the data record. The latter result indicates that the flow does not follow the short term fluctuations in the cylinder frequency, which are comparable to the spectral resolution.

One of the drawbacks of periodic sampling methods such as the multichannel

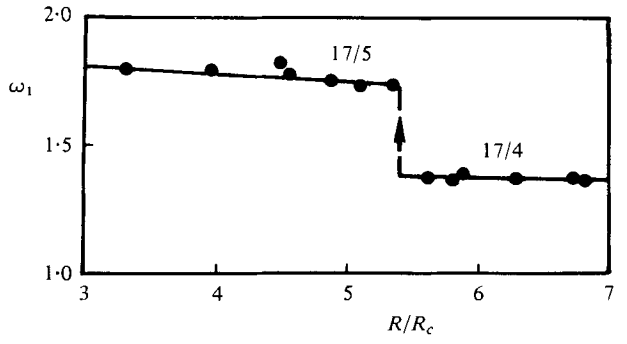

FIGURE 4. The discontinuous variation of the azimuthal wave frequency when the number of azimuthal waves changes from 4 to 5 as the Reynolds number is decreased through $R/R_c = 5{\cdot}4$ for the state with 17 axial vortices. The wave frequency ω_1 jumps from 1·38 to $\frac{5}{4} \times 1{\cdot}38 = 1{\cdot}73$.

frequency counting scheme that we have used is that spectra obtained for the range 0 to ω_N contain 'aliases', which are higher frequency components folded into the 0 to ω_N range (Otnes & Enochson 1978). An example is shown in figure 3(*b*), which shows a spectral component called ω_1 and aliases of two of its harmonics. The aliases can be identified by comparing two spectra obtained with different sampling times. For each fluid flow condition we always obtain two spectra, usually with sampling times for which $\omega_N = 2$ and $\omega_N = 20$. (Frequencies in this paper are expressed in units of the cylinder frequency; hence they are dimensionless.)

3.5. *Choice of spatial state*

At a given Reynolds number there are several distinct stable spatial states which can be obtained, depending on the Reynolds number history of the system (see § 2.5). Early in the present study it was established that different states p/m have somewhat different spectra and transition Reynolds numbers. Therefore, it became clear that a study of the transitions of a fluid flow would be meaningful only if the spatial state were determined for every spectral measurement. However, a detailed study of the dynamical behaviour of every accessible spatial state and of the transitions between the variety of different spatial states was obviously not possible in a reasonable length of time. On the other hand, the stability of a spatial state suggested that while different states may be nearly degenerate in energy, they are separated by a potential barrier of reasonable height, making it unlikely that the non-uniqueness of a spatial state is related to the dynamics of the transition to turbulence. Therefore, we conjectured that the Reynolds number dependence could be factored effectively into two separate problems, the first being the dependence of the spatial state on the Reynolds number history and the second being the transition to turbulence under quasistatic changes in Reynolds number for a given spatial state. We have studied the latter problem.

The spatial state with 17 axial vortices and (where the waves exist) four azimuthal waves was arbitrarily selected for detailed study. This state was produced about 25 % of the time by rapidly accelerating the system from rest to $R/R_c \simeq 10$; when this procedure yielded states other than 17/4 state, the system was re-started repeatedly until the 17/4 state was produced. Once it is produced the 17 vortex state is stable under quasistatic changes in Reynolds number from $R/R_c = 5{\cdot}4$ to beyond $R/R_c = 45$ (the

largest Reynolds number studied). As the Reynolds number is decreased below $R/R_c = 5{\cdot}4$, the 17/4 state loses stability to the 17/5 state, as shown in figure 4. For $5{\cdot}4 < R/R_c < 21{\cdot}9$ the 17/4 state remains unchanged unless R is changed very rapidly. The 4 azimuthal waves disappear at $R/R_c = 21{\cdot}9$, but the 17 vortices persist to the largest Reynolds number studied. If the Reynolds number is lowered again below $R/R_c = 21{\cdot}9$, the 4 azimuthal waves reappear. Although our measurements were made primarily on the 17/4 state, a few measurements were made on other states (see §4.2).

4. Experimental results

This section presents first the principal results and then other results, and concludes with a summary of the experimental observations. Preliminary results from these experiments were reported in Gollub & Swinney (1975); Swinney, Fenstermacher & Gollub (1977*a*, *b*); Fenstermacher *et al.* (1979); Swinney & Gollub (1978).

4.1. *Principal results*

The radial component of the velocity was measured as a function of time in the range $5{\cdot}4 < R/R_c < 45$ for the state with 17 vortices and (where they exist) 4 azimuthal waves. For most measurements the scattering volume was located midway between the inner and outer cylinders, usually at a distance one-eighth of an axial wavelength below an outflow boundary of a vortex located near the axial centre; however, velocity power spectra obtained at other radial positions and heights in the annulus contain the *same* frequency components.

Figure 5 shows velocity records and velocity fluctuation power spectra representative of those obtained in the Reynolds number range studied, and figure 6 (plate 2) shows photographs of the flow at essentially the same Reynolds numbers. The velocity graphs in figure 5 are short segments of records that contain typically 1500 oscillations. The time and frequency scales in the figures are in units of the inner cylinder rotation period and frequency, respectively, and the power spectra are normalized so that

$$\int_0^{\omega_N} P(\omega)\, d\omega = \langle (\Delta V_r)^2 \rangle.$$

Velocity spectra extending to higher frequencies than those in figure 5 contain no fundamental frequency components not shown in figure 5.

Above the transition at $R/R_c = 1{\cdot}2$ from time-independent Taylor vortex flow to time-dependent wavy vortex flow the velocity power spectra contain a single frequency component which corresponds to the azimuthal waves passing the point of observation; we call this frequency ω_1. An example of a velocity graph and the power spectrum for the 17 vortex 4 wave state in this regime is shown in figure 5(*a*), and figure 6(*a*) is the corresponding flow photograph. Power spectra extending to higher frequencies contain many harmonics of ω_1, as figure 7(*a*) illustrates; figure 1(*b*) is the flow photograph corresponding to figure 7(*a*). Note in figures 1(*b*) and 6(*a*) the phase angle between the waves on the inflow and outflow boundaries, and the absence of small scale structure. The amplitude of the component at ω_1 is 5 orders of magnitude above the instrumental noise background. The linewidth of ω_1 is equal to that of a sine

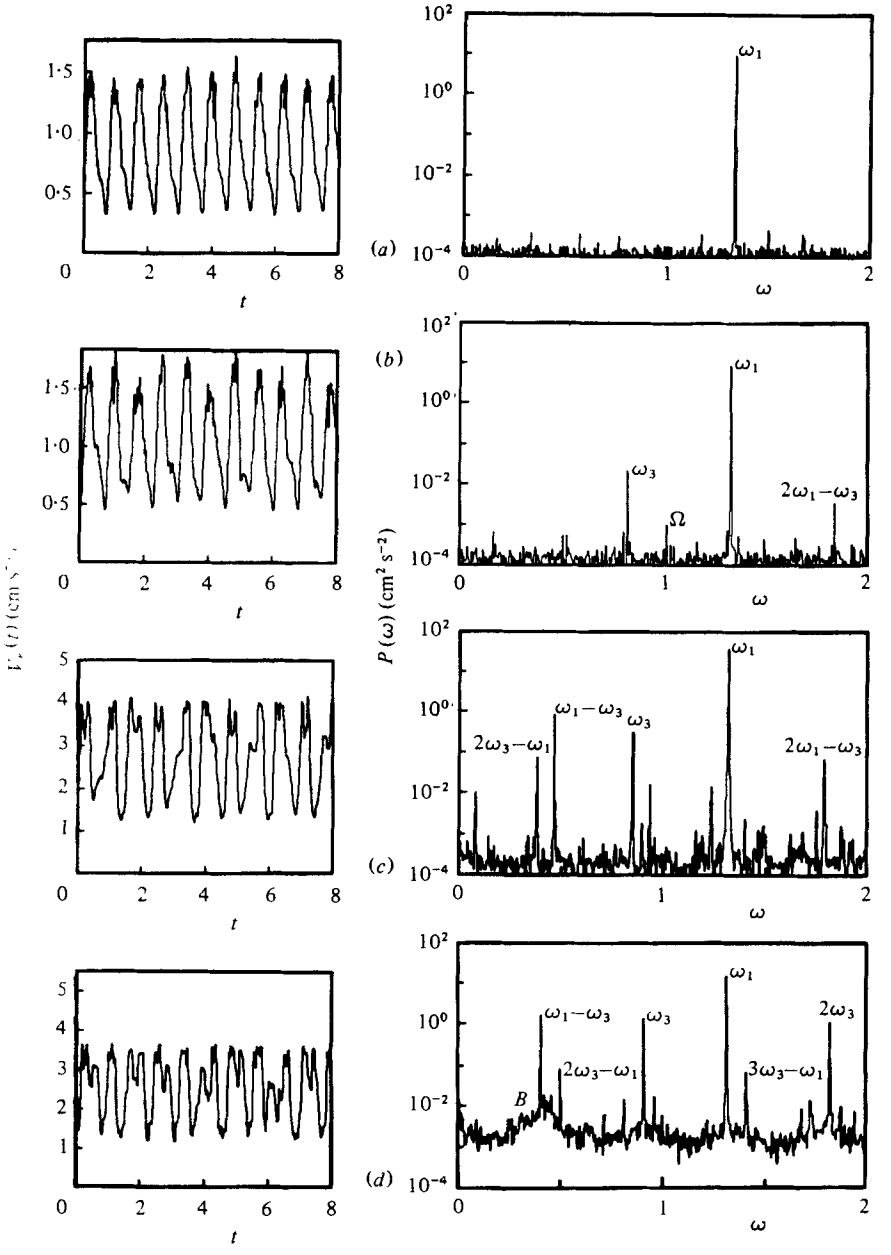

FIGURE 5 (*a–d*). For legend see next page.

wave sampled for the same period of time (see § 3.4); hence within the accuracy of the measurement the flow in this regime is strictly periodic.

The second fundamental frequency component of the steady-state flow appears at $R/R_c = 10{\cdot}06$. We call this component ω_3; a transient component called ω_2 will be discussed in § 4.2. The component ω_3 can be seen in the velocity spectra in figures 5 (*b*)–(*e*). The corresponding photographs of the flow, figures 6 (*b*)–(*e*), show a gradual increase in the small scale structure of the flow pattern, but we have not been able to

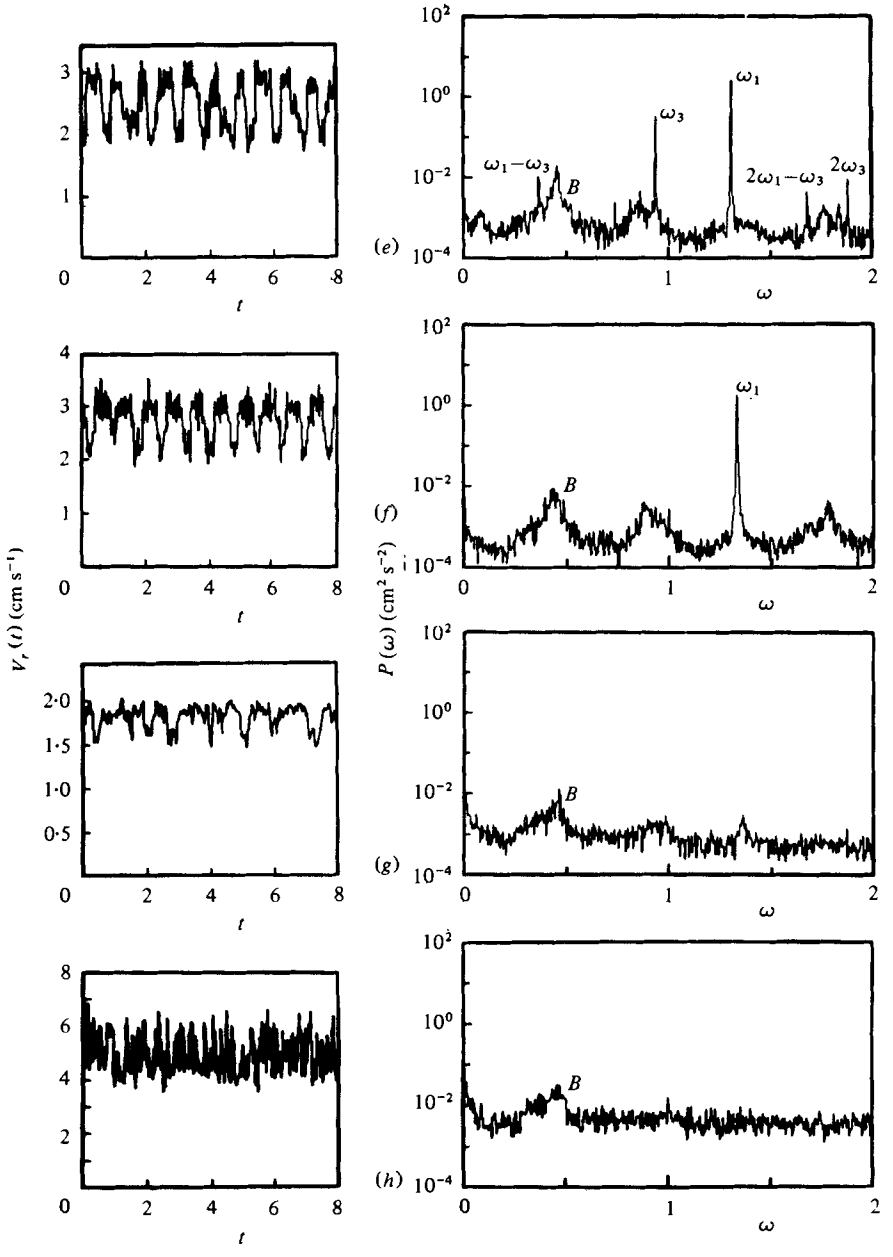

FIGURE 5. The time-dependence of the radial velocity component and the corresponding velocity fluctuation power spectra for a flow in a concentric cylinder system with specifications as given in table 1. R/R_c values: (*a*) 9·6; (*b*) 10·1; (*c*) 11·0; (*d*) 15·1; (*e*) 18·9; (*f*) 21·7; (*g*) 23·0; (*h*) 43·9. The corresponding photographs of the flow are in figure 6. These data were obtained for water at 27·5 °C except (*g*) which was obtained at 60 °C. In terms of the dimensionless time t and frequency ω of the graphs (see text) the time in seconds is given by $4{\cdot}328t/(R/R_c)$ and the angular frequency in radians/s by $1{\cdot}452\omega(R/R_c)$, except for (*g*) where the times (frequencies) are larger (smaller) by a factor of 1·71 because of the smaller viscosity at the higher temperature. The smaller viscosity is the main reason that the velocities in (*g*) are smaller than in (*f*) or (*h*).

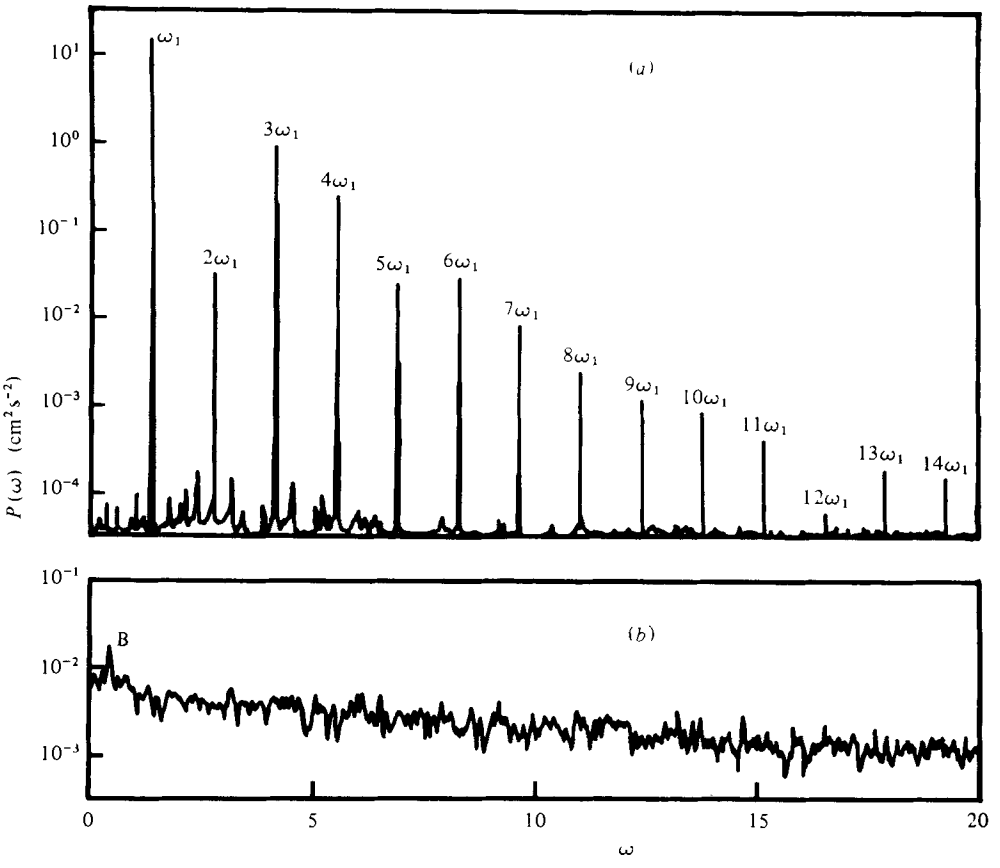

FIGURE 7. Power spectra of the radial velocity component for flow between concentric cylinders in the system described in table 1. The spectrum in (*a*) corresponds to the flow pictured in figure 1(*b*), and (*b*) corresponds to that pictured in figure 6(*h*). (*a*) $R/R_c = 5{\cdot}6$. (*b*) $R/R_c = 44{\cdot}0$.

identify any particular feature in the flow photographs with the mode at frequency ω_3.† However, the spectral power of the component at ω_3 is typically two or more orders of magnitude less than that of ω_1, so, unless ω_3 is appreciably stronger in another coordinate direction, it may be difficult to observe by flow visualization.

The appearance of ω_3 at $R/R_c = 10{\cdot}06$ has been reproducible to better than 1 % in experiments over a two year period. Within the experimental uncertainty there is no hysteresis: ω_3 appears at $R/R_c = 10{\cdot}06$ with increasing Reynolds number and disappears at the same R/R_c as the Reynolds number is decreased. After its onset this mode grows in amplitude, reaches a maximum, and then declines until it disappears at $R/R_c = 19{\cdot}3 \pm 0{\cdot}2$. The latter is also a non-hysteretic transition. No broadening of ω_3 beyond the instrumental linewidth was observed.

The first chaotic element in the flow appears within the regime in which both ω_1 and ω_3 are present, at $R/R_c \simeq 12$, where a broad weak component is observed at a frequency approximately one-third of the wave frequency ω_1. This component, labelled B in figures 5(*d*)–(*h*), has an onset which is difficult to determine accurately because the component is weak and the background continuum level is somewhat different for different sets of data; moreover, the onset of B may have some hysteresis.

† See note added in proof on p. 126.

Above $R/R_c = 19{\cdot}3$, where ω_3 disappears, the spectrum contains only ω_1 and B and their harmonics, as shown in figure 5(*f*). With a further increase in Reynolds number the intensity of the component at ω_1 gradually decreases, and at $R/R_c = 21{\cdot}9 \pm 0{\cdot}2$ the sharp component at ω_1 disappears from the spectrum, although a broad weak feature remains, as in figure 5(*g*). The disappearance of ω_1 corresponds to the disappearance of the azimuthal waves, which can easily be seen in the flow visualization (cf. figures 6*f*, *g*). The disappearance of ω_1 is especially dramatic in graphs of the velocity fluctuation autocorrelation function, $\langle \Delta V_r(t)\, \Delta V_r(t+\tau)\rangle$, which oscillates for all τ for $R/R_c < 21{\cdot}9$ but decays for larger Reynolds number (Swinney, Fenstermacher & Gollub 1977*b*). Although the velocity fluctuations become completely uncorrelated at long times for $R/R_c > 21{\cdot}9$, this Reynolds number should not be identified as the onset of chaotic flow. The flow begins to become disordered at much smaller Reynolds number, $R/R_c \simeq 12$, as is marked by the appearance of B and the increasing small scale structure in the photographs.

As the Reynolds number is increased further the background continuum level gradually increases, as shown for $R/R_c = 43{\cdot}9$ in figures 5(*h*) and 7(*b*), but no further transitions are observed. Although the spectrum at large Reynolds number has no sharp peaks, this does not imply that the flow is totally featureless. Figures 1(*d*) and 6(*g*) clearly illustrate that the vortices persist. The velocity fluctuation autocorrelation function decays, but measurements of the time-average of the velocity field reveal the presence of the vortex structure.

Some general remarks regarding the velocity records and spectra are in order before describing other results and summarizing the observations:

(1) The frequencies ω_1, ω_3, and B are independent of r and z at a given Reynolds number, but the intensities of these components and their harmonics depend on r and z; for example, as would be expected, if the probe volume is at a vortex boundary the intensity of the component at $2\omega_1$ is greater than that of ω_1, while for a probe volume positioned away from a vortex boundary the second harmonic is weaker than the fundamental (as in figure 7*a*).

(2) The component ω_1 dominates the spectra throughout the wavy vortex flow regime. The components ω_3 and B and their harmonics are easily observed in the logarithmic power spectra because of the high signal-to-noise ratio, but the integrated power of these components is down by an order of magnitude or more from that of ω_1.

(3) No sharp fundamental frequency components were observed for the steady-state flow other than ω_1 and ω_3. *All* other sharp components are given by $n\omega_1 + q\omega_3$, where n and q are integers. A few of these components are labelled in figures 5(*b*)–(*e*).

(4) The velocity has a decreasing modulation depth and becomes increasingly noisy as the Reynolds number is increased (figure 5). This coincides with the increasing small scale structure in the flow photographs (figure 6).

(5) The noise in the velocity records contributes to the background continuum in the velocity spectra. For spectra in the same data set the background level increases monotonically with increasing Reynolds number; however, the background level at a given R varies slightly from one data set to another due to small differences in the adjustment of the optics and electronics. Thus, for example, the background in 5(*e*) is smaller than in 5(*d*), but these spectra are from different data sets, while, for (*c*) and (*d*) which are from the same data set, the background level increases with increasing R.

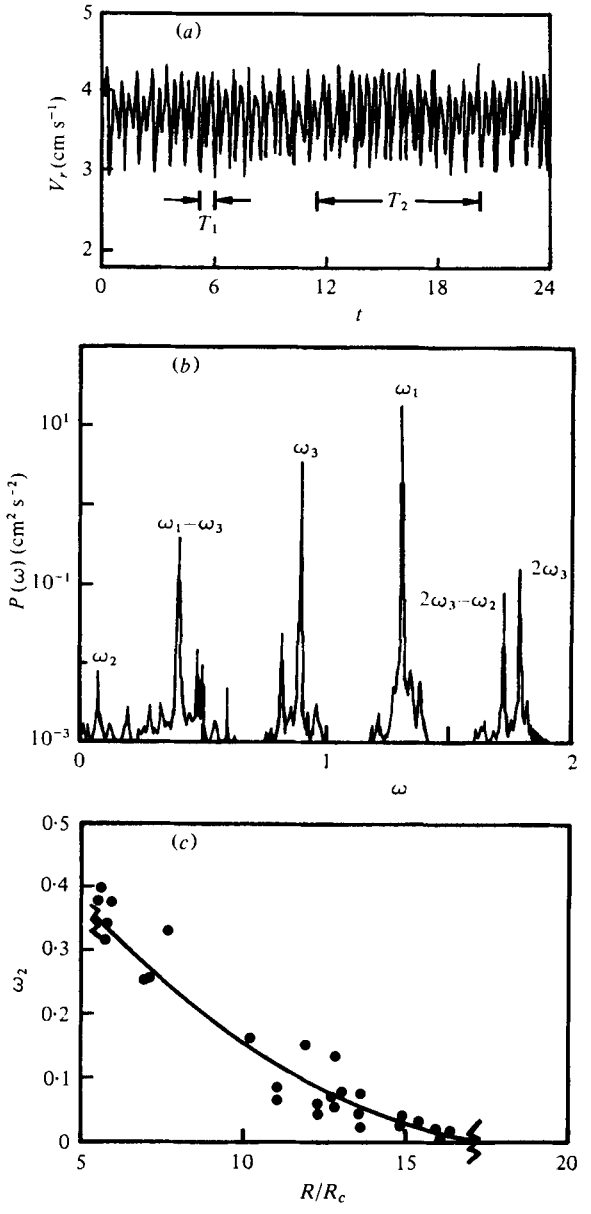

FIGURE 8. These data illustrate the characteristics of the transient mode ω_2. (*a*) A portion of a velocity record obtained at $R/R_c = 13{\cdot}0$. The times T_1 and T_2 are respectively the periods of the components with frequencies ω_1 and ω_2. (*b*) The power spectrum corresponding to the velocity record in (*a*). (*c*) Dependence of ω_2 on Reynolds number.

4.2. *Other results*

In some of the runs we have observed a low frequency component which we call ω_2 because it first appears if at all at Reynolds numbers intermediate between the appearance of ω_1 and ω_3. When present the ω_2 mode was quite evident in the velocity record, as figure 8(*a*) illustrates, and could be seen as a sharp spectral component in

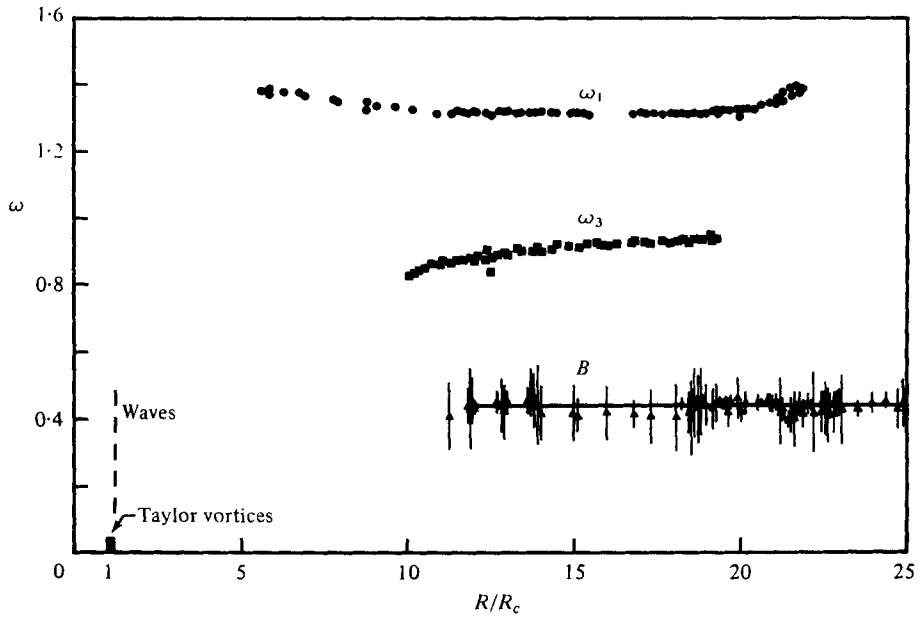

FIGURE 9. The fundamental frequency components observed in the power spectra of the radial velocity component for a flow with 17 vortices and, in the range where the waves exist, 4 waves. The wave frequency is ω_1. No sharp spectral components were observed above $R/R_c = 21{\cdot}9$. The triangular points and vertical bars indicate respectively the centre frequency and linewidth (FWHM) of the broad component B; the horizontal bar is its average centre frequency.

the velocity spectrum, as in figure 8(*b*). This mode was usually absent but could be produced fairly reliably by rapid starts to R/R_c between about 8 and 12. It lasted from a few seconds to as long as two hours, but it was always found to decay. The frequency ω_2 was not accurately reproducible, but on the average it decreases to zero with increasing Reynolds number (figure 8*c*).

In addition to the studies on the 17/4 state described in the previous subsection, a brief survey of the 15/4 state was made (see Swinney *et al.* 1977*a*). Both the 15 and 17 vortex states are stable as the Reynolds number is changed in either direction throughout the range $6 \lesssim R/R_c \lesssim 45$. Furthermore, the same spectra were obtained for a given spatial state independently of the way in which the state was achieved. Flow visualization studies indicate that the stability of the spatial state is a property of the relatively short fluid height to gap ratio; for large heights there are more accessible states and more transitions between them.

4.3. *Summary of the results*

Figure 9 shows the Reynolds number dependence of the fundamental frequency components ω_1, ω_3, and B observed for the steady flow; all the transitions involving these modes are listed in table 2. The components ω_3 and B and the transient component ω_2 have not been observed prior to the present work. Unlike the azimuthal wave frequency ω_1, the modes ω_2, ω_3 and B have not been identified with any feature in the flow photographs.

The frequency ω_3 increases monotonically with increasing R, while ω_1 is fairly

Relative Reynolds number, R/R_c	Transition	Frequency components†	Dynamical regime
1·0	Taylor vortex flow	None	Time-independent
1·2‡	Wavy vortex flow	ω_1	Periodic
$10{\cdot}1 \pm 0{\cdot}1$	ω_3 appears	ω_1, ω_3	Quasi-periodic
~ 12	B appears	ω_1, ω_3, B	Weakly turbulent with sharp spectral components
$19{\cdot}3 \pm 0{\cdot}2$*	ω_3 disappears	ω_1, B	Weakly turbulent with sharp spectral components
$21{\cdot}9 \pm 0{\cdot}2$*	ω_1 disappears	B	Weakly turbulent

† These frequencies characterize the steady-state flow. The component ω_2 is a transient (see §4.2).

‡ Cole (1976).

* These Reynolds numbers are 2·4 % smaller than those reported by Swinney, Fenstermacher & Gollub (1977*a*, *b*) and Fenstermacher *et al.* (1979) owing to an error in the viscosity value used in the earlier calculation of R. The cylinder frequencies for the transitions are the same as reported previously.

TABLE 2. Transitions in the flow between concentric cylinders for the system with specifications given in table 1.

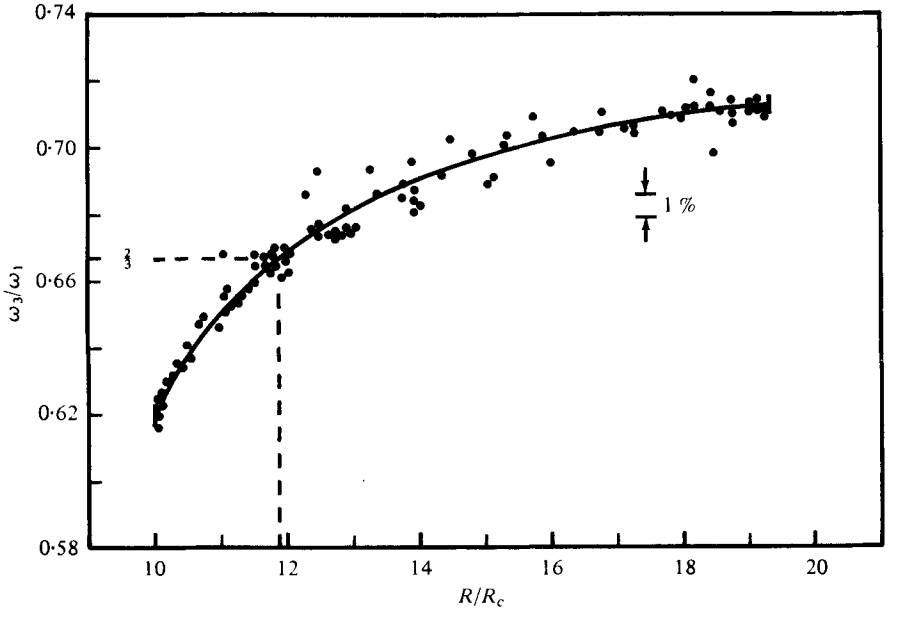

FIGURE 10. The dependence of ω_3/ω_1 on Reynolds number in the regime where ω_3 was observed. The significance of $\omega_3/\omega_1 = \frac{2}{3}$ is discussed in §6.4.

constant, increasing slightly at the ends of the Reynolds number range where this mode exists. Within the experimental uncertainty the ratio ω_3/ω_1 increases continuously and monotonically with increasing R, as shown in figure 10. Therefore, the

ratio ω_3/ω_1 is in general irrational and the regime with the two modes ω_3 and ω_1 is then quasi-periodic.

The frequency of the broad mode appears to be independent of Reynolds number; it is $0{\cdot}44 \pm 0{\cdot}02$ (standard deviation). This spectral component was too noisy and weak to determine its lineshape. Its full-width at half-maximum varied from 0·01 to 0·2 in measurements at the same Reynolds number, as figure 9 illustrates; the average value was 0·05. There was no apparent systematic variation with Reynolds number.

5. Comparison with other experiments

Figure 6 illustrates the increasing small scale structure in the flow and the disappearance of the azimuthal waves with increasing Reynolds number, as observed in previous photographic studies. The only result of the present experiment for which there is a quantitative previous observation is the measurement of the Reynolds number dependence of the wave frequency ω_1. Coles (1965, figure 6) found ω_1/m to be a universal function of Reynolds number, independent of the spatial state. Our measurements of ω_1, including data (not shown) which extend down to the onset of the wavy regime, are in general agreement with the Reynolds number dependence observed by Coles, but we note that ω_1/m at a given Reynolds number can differ by a few per cent for different spatial states (see Swinney *et al.* 1977*a*, figure 8).

Recent experiments on time-dependent Taylor vortex flow by Walden & Donnelly (1979) using entirely different experimental methods (Donnelly, 1965) are in agreement with the sequence of time-dependent phenomena described in this paper. In addition, they find that for fluid height to gap ratios greater than 25 another sharp component appears in the power spectrum in the Reynolds number range $28 \lesssim R/R_c \lesssim 36$.

A sequence of instabilities quite similar to that described in this paper has been observed by Gollub & Benson (1978) in a laser-Doppler velocimetry study of Rayleigh–Bénard convection. In particular, the velocity spectra show a periodic regime with a single fundamental frequency followed by a quasiperiodic regime with two fundamental frequencies, and then broadband noise components appear in the spectra; finally, the sharp frequency components disappear.

The sequence of instabilities observed in these studies is certainly not the only one possible. It is of course very well known that many flows make a direct transition from laminar to turbulent flow. Even in the Taylor and the Rayleigh–Bénard geometries the transitional behaviour with different geometrical parameters can be quite different from that we have described. For example, Ahlers & Behringer (1978) have discovered that in Rayleigh–Bénard convection in a fluid container with a relatively large ratio of the diameter to height (= 57), broadband noise occurs in the heat flux just above the onset of convection; there is no periodic regime at all. This dependence of even the qualitative features of the transition process on a geometrical variable does not offer much encouragement for efforts to construct general models for the transition to turbulence.

6. Discussion

Fluid flows are often said to be characterized by one or more discrete frequencies, but the experimental evidence supporting this picture is limited. Our velocity power spectra provide the strongest evidence of which we are aware for the existence of strictly periodic and quasi-periodic regimes in a fluid flow.

The principal finding of this work is that periodic wavy vortex flow is followed by only one additional distinct dynamical regime (quasi-periodic flow with two frequencies) prior to the appearance of a chaotic flow. The appearance of the broad spectral peak, which is the hallmark of a chaotic flow, represents a profound change in the mathematical description of the system, but the quantitative change is initially small; thus, for example, the broad peak in figure 5(*d*) contains less than one per cent of the total spectral energy.

6.1. *The Landau picture*

Years ago Landau (1944; Landau & Lifshitz 1959) conjectured that the transition to turbulence would occur as an infinite sequence of hydrodynamic instabilities, each adding a new frequency to the motion. His idea was that successive instabilities could be found by a repeated application of linear stability analysis. The flow becomes 'complicated and confused' as more, generally incommensurate, frequencies are added to the motion, but in this view there is no well-defined onset of turbulence. Even at large R the flow is quasi-periodic rather than chaotic.

Long sequences of hydrodynamic instabilities resulting in quasi-periodic motion characterized by many frequencies have never been observed, but there have been few experiments that could distinguish between genuinely chaotic flows and complex quasi-periodic ones. In the system studied here the flow is characterized by not more than two sharp frequency components at any Reynolds number, and it becomes chaotic after a small number of instabilities. These observations are contrary to Landau's conjecture.

6.2. *Dynamical systems*

A seminal paper by Ruelle & Takens (1971) has stimulated extensive research using dynamical systems theory to study the transition to turbulence. In this approach the 'generic' (typical) properties of the solutions of nonlinear ordinary differential equations are studied geometrically and qualitatively; partial differential equations such as the Navier–Stokes equations are assumed to exhibit similar behaviour.

We will describe the transitions in the Taylor vortex flow system using the language of dynamical systems in order to indicate how a theorem of Newhouse, Ruelle and Takens (1978) may relate to our observations. The discussion will be non-rigorous and speculative; no attempt will be made to define explicitly all terms. The monographs of Hirsch & Smale (1974), Marsden & McCracken (1976) and Teman (1976) should be consulted for expositions of dynamical systems theory.

The behaviour of a nonlinear system can be described in terms of the trajectories of the solutions in a phase space. One way to construct a co-ordinate representation of this space is to expand the velocity field $\mathbf{V}(\mathbf{r}, t)$ in a complete set of eigenfunctions $\mathbf{U}_n(\mathbf{r})$:

$$\mathbf{V}(\mathbf{r}, t) = \Sigma a_n(t)\, \mathbf{U}_n(\mathbf{r}).$$

Then in the space spanned by the $\mathbf{U}_n$ the system at any instant in time is prescribed by the point with co-ordinates $\{a_n(t)\}$. The set of all trajectories corresponding to different initial conditions at a given Reynolds number form a phase portrait of the system. Many theorems of dynamical systems are stated in terms of the topology of these phase portraits.

The azimuthal flow at small Reynolds number is characterized by a stable fixed point in phase space. This point is globally attracting; thus, regardless of the initial conditions, the phase space trajectory will approach asymptotically this fixed point. Time-independent Taylor vortex flow is also described by an attracting fixed point. However, beyond R_c the number of axial vortices is not unique (Snyder 1969*b*), so there must be several stable fixed points in the phase space, each with its own basin of attraction. The particular fixed point approached asymptotically depends on the initial conditions.

At the transition to wavy vortex flow the fixed point becomes unstable and the new stable attractor is a limit cycle, a closed loop in phase space. Topologically the limit cycle is described as a one-dimensional torus, T^1, embedded in the infinite-dimensional phase space.

The next dynamical regime is a quasi-periodic flow with two frequencies, ω_1 and ω_3. The limit cycle becomes unstable and the new stable attractor is a quasi-periodic flow on a torus T^2, a closed two-dimensional surface. If the ratio ω_3/ω_1 were rational, the asymptotic trajectory would be a closed orbit on the torus, but, because the ratio appears to be irrational, the trajectory never repeats itself. However, the orbits are stable in the sense that, if two orbits are initially close together, they will remain close together for all time.

In the Landau picture the next transition would be to a quasiperiodic regime characterized by three frequencies, and the attractor would be a quasi-periodic flow on a three-dimensional torus, T^3. This is not observed. Instead of a regime with three discrete frequencies, we find that a broad peak appears, marking the onset of a qualitatively different kind of behaviour. The trajectories in phase space are attracted toward a subspace on which they wander erratically *ad infinitum*. Such a subspace is called a 'strange attractor'. There is now a sensitive dependence on initial conditions; no matter how close together two orbits are initially, they will eventually wander apart.

Now we can relate the experimental observations to the theorem of Newhouse, Ruelle & Takens (1978). The theorem states in part (paraphrasing): in every suitably differentiable neighbourhood of a vector field on the torus T^m there is a vector field having a strange attractor if $m \geqslant 3$. Although there may also be nearby periodic orbits for $m \geqslant 3$, the theorem suggests that turbulence may arise from infinitesimal perturbations of a quasi-periodic flow on T^3; hence a quasi-periodic flow with three frequencies may be unobservable.

Our results for time-dependent Taylor vortex flow appear to be consistent with the predictions of Newhouse *et al.* That is, the flow characterized by two discrete frequencies makes a transition to a chaotic flow rather than to a quasi-periodic flow with three frequencies. However, Ruelle (private communication) has pointed out that since the azimuthal wave frequency ω_1 could be removed from the spectra by a transformation to a rotating co-ordinate system, the flow could be viewed as characterized by a single fundamental frequency (ω_3) before becoming turbulent.

It should be reiterated that, at the present stage of development of dynamical

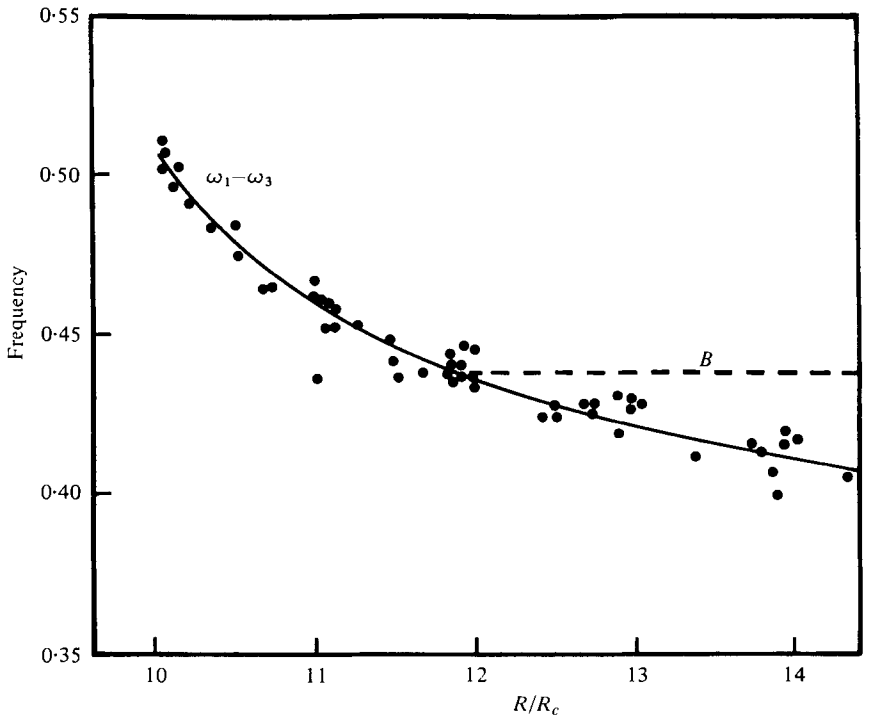

FIGURE 11. This graph supports the conjecture that the broadband component B is excited by the component at $\omega_1-\omega_3$, since B is first observed at $R/R_c \simeq 12$, where $\omega_1-\omega_3 = B$.

systems theory, its relation to fluid mechanics should be considered as suggestive rather than conclusive. Nevertheless, it is notable that while many flows are characterized by fewer than two frequencies before they become turbulent (§5), none of the flows that have been studied (to our knowledge) are described asymptotically by more than two discrete frequencies. This appears to support the applicability of the Newhouse–Ruelle–Takens theorem.

6.3. *Finite models*

Since the solution of the Navier–Stokes equations for instabilities beyond the first one or two is not possible with current mathematical techniques, an alternative approach that has been pursued by many workers in recent years is the use of numerical analysis to study models with a few degrees of freedom. The classic prototype for such studies is the three-variable model of convection which Lorenz (1963) discovered has chaotic dynamics. This discovery demonstrates that only three degrees of freedom are needed to produce chaotic behaviour, and it has led to the conjecture that turbulence in a fluid flow at large Reynolds numbers where many degrees of freedom are excited may not be qualitatively different from chaos in a system with a few degrees of freedom. Thus it is hoped that the simple models with a few degrees of freedom may exhibit the qualitative behaviour of real fluid flows.

The velocity spectra and photographs for Taylor vortex flow indicate that only a few degrees of freedom may be excited up to $R/R_c \simeq 12$, but the presence of the broad peak B and the small scale structure visible in the photographs are evidence that many degrees of freedom are excited at larger Reynolds number.

Sherman & McLaughlin (1978) constructed a model with only 5 coupled modes. The mode frequencies were assumed rather than calculated and the z dependence was neglected. It was found that, as the growth rate of the modes was increased, there was a transition from a power spectrum with sharp components to one with broad components similar to the one we have called B.

A much more realistic model of Taylor vortex flow was considered by Yahata (1978). The z dependence was described by a single sinusoidal mode and the azimuthal dependence by the mean flow and a sinusoidal mode corresponding to 4 waves. Retaining more modes in the radial direction, Yahata obtained a set of 32 coupled amplitude equations. Power spectra of the radial component of the velocity showed: for $R/R_c = 7{\cdot}97$, a single sharp frequency component, which presumably corresponds to ω_1; for $R/R_c = 15{\cdot}97$, two components corresponding approximately to ω_1 and ω_3; for $R/R_c = 22{\cdot}31$, the component at ω_3 had disappeared while the component at ω_1 remained intense; and for $R/R_c = 23{\cdot}91$ the component at ω_1 had become broad. The behaviour of this model is very similar to that observed in the experiment except for the experimental observation of the broad component B.

Curry (1978) has studied a model of convection with 14 modes and has found that it has successive regimes that are periodic, quasi-periodic with two frequencies, and chaotic; thus the model's dynamical behaviour is similar to that observed in our experiments on Taylor vortex flow. Another feature found for this model that is common with the observations for Taylor vortex flow is non-uniqueness (hysteresis), which for the model means that there are several attracting sets in phase space at the same Rayleigh number.

One aspect of our observations that is not exhibited by these or other nonlinear models studied thus far is the simultaneous occurrence of broad and sharp frequency components. Further studies of nonlinear models should help guide future experiments and yield insight into the transition to turbulence problem.

6.4. *Excitation of the broad component*

A possible source of the excitation of the broad component in our spectra is the component with frequency equal to $\omega_1 - \omega_3$. Within the experimental uncertainty, the broad component appears when $\omega_1 - \omega_3 = B$, where B is the centre frequency of the broad peak. This frequency matching condition is satisfied at $R \simeq 12$, as shown in figure 11. It is tempting to speculate that the noise component is being excited by the nonlinear interaction between the modes with frequencies ω_1 and ω_3.

Another possible explanation of the appearance of B has been suggested by Bowen (1977). His argument is based on the observation that the trajectory of the system in phase space could change topological type when the frequencies ω_1 and ω_3 become commensurate. When the frequencies are incommensurate the phase space trajectory fills the surface of a torus, whereas when the frequencies become commensurate the trajectories could collapse to a single closed curve on the torus. Although the rational numbers are dense in the reals, the preference for small integer ratios leads to the choice $\omega_3/\omega_1 = \frac{2}{3}$ as the value of the frequency ratio where the chaotic mode would appear. Figure 10 shows that this value of the ω_3/ω_1 ratio is reached when $R/R_c = 11{\cdot}9 \pm 0{\cdot}4$, which is indeed equal within the experimental uncertainty to

the Reynolds number corresponding to the appearance of B. However, the uncertainties are large and the agreement may well be accidental.

6.5. *Concluding remarks*

The study of the transition to turbulence is motivated in part by the hope that general models of transition can be developed. The present and other (§ 5) experiments and the numerical analyses of nonlinear models indicate that chaotic behaviour occurs after at most a small number of transitions to distinct regimes. However, the processes are certainly different for different systems. For example, in channel flow there is a direct transition to turbulence, while in the system we have studied there are four distinct regimes (two time-independent and two time-dependent) preceding turbulence. Clearly much additional research will be necessary to determine if hydrodynamic flows can be grouped into a small number of classes in which the behaviour is qualitatively similar.

Note added in proof, July 1979. In recent experiments at The University of Texas, M. A. Gorman in collaboration with H. L. Swinney has identified the ω_3 mode as a modula- of the ω_1 mode. The frequencies of the ω_1 and ω_3 modes were determined over a range of Reynolds numbers by flow visualization techniques for states with $m = 3$, 4, 5 and 6 in an apparatus ($r_0 = 5{\cdot}95$ cm; $r_i/r_0 = 0{\cdot}833$) with height to gap ratios ranging from 16 to 42.

This work was supported by National Science Foundation Grants DMR76-11033 and ENG76-19810 to City College of the City University of New York. We are grateful to Robert Tsang for his assistance in the analysis of the data. We have benefited greatly from discussions with many colleagues, including D. Coles, R. C. DiPrima, R. J. Donnelly, D. D. Joseph, E. L. Koschmieder, J. B. McLaughlin, P. C. Martin, D. Ruelle, D. J. Tritton and J. Yorke.

REFERENCES

AHLERS, G. & BEHRINGER, R. 1978 Evolution of turbulence from the Rayleigh–Bénard instability. *Phys. Rev. Lett.* **40**, 712–716.

BENJAMIN, T. B. 1978 Bifurcation phenomena in steady flows of a viscous fluid. I. Theory, II. Experiments. *Proc. Roy. Soc.* A **359**, 1–26; 27–43.

BOWEN, R. 1977 A model for Couette flow data. In *Berkeley Turbulence Seminar*, Springer Lecture Notes in Mathematics no. 615, pp. 117–134.

BURKHALTER, J. E. & KOSCHMIEDER, E. L. 1973 Steady supercritical Taylor flows. *J. Fluid Mech.* **58**, 547–560.

BURKHALTER, J. E. & KOSCHMIEDER, E. L. 1974 Steady supercritical Taylor vortices after sudden starts. *Phys. Fluids* **17**, 1929–1935.

COLE, J. A. 1976 Taylor-vortex instability and annulus-length effects. *J. Fluid Mech.* **75**, 1–15.

COLES, D. 1965 Transition in circular Couette flow. *J. Fluid Mech.* **21**, 385–425.

COUETTE, M. 1890 Études sur le frottement des liquides. *Ann. Chimie Phys.* (21) **6**, 433–510.

CURRY, J. H. 1978 A generalized Lorenz system. *Commun. Math. Phys.* **60**, 193–204.

DAVEY, A. 1962 The growth of Taylor vortices in flow between rotating cylinders. *J. Fluid Mech.* **14**, 336–368.

DAVEY, A., DIPRIMA, R. C. & STUART, J. T. 1968 On the instability of Taylor vortices. *J. Fluid Mech.* **31**, 17–52.

DIPRIMA, R. C. & EAGLES, P. M. 1977 Amplification rates and torques for Taylor-vortex flows between rotating cylinders. *Phys. Fluids* **20**, 171–175.

DONNELLY, R. J. 1958 Experiments on the stability of viscous flow between rotating cylinders. I. Torque measurements. *Proc. Roy Soc.* A **246**, 312–325.

DONNELLY, R. J. 1963 Experimental confirmation of the Landau law in Couette flow. *Phys. Rev. Lett.* **10**, 282–284.

DONNELLY, R. J. 1965 Experiments on the stability of viscous flow between rotating cylinders. IV. The ion technique. *Proc. Roy. Soc.* A **283**, 509–519.

DONNELLY, R. J. & SCHWARZ, K. W. 1965 Experiments on the stability of viscous flow between rotating cylinders. VI. Finite-amplitude experiments. *Proc. Roy. Soc.* A **283**, 531–556.

DONNELLY, R. J. & SIMON, N. J. 1960 An empirical torque relation for supercritical flow between rotating cylinders. *J. Fluid Mech.* **7**, 401–418.

DURRANI, T. S. & GREATED, C. A. 1977 *Laser Systems in Flow Measurements*. New York: Plenum.

EAGLES, P. M. 1971 On stability of Taylor vortices by fifth-order amplitude expansions. *J. Fluid Mech.* **49**, 529–550.

EAGLES, P. M. 1974 On the torque of wavy vortices. *J. Fluid Mech.* **62**, 1–9.

FENSTERMACHER, P. R., SWINNEY, H. L., BENSON, S. A. & GOLLUB, J. P. 1979 Bifurcations to periodic, quasiperiodic, and chaotic regimes in rotating and convecting fluids. *Ann. N.Y. Acad. Sci.* **316**, 652–666.

GOLLUB, J. P. & BENSON, S. V. 1978 Chaotic response to periodic perturbation of a convecting fluid. *Phys. Rev. Lett.* **41**, 948–951.

GOLLUB, J. P. & FREILICH, M. H. 1976 Optical heterodyne test of perturbation expansions for the Taylor instability. *Phys. Fluids* **19**, 618–625.

GOLLUB, J. P. & SWINNEY, H. L. 1975 Onset of turbulence in a rotating fluid. *Phys. Rev. Lett.* **35**, 927–930.

HIRSCH, M. W. & SMALE, S. 1974 *Differential Equations, Dynamical Systems, and Linear Algebra. New York: Academic Press.*

KOSCHMIEDER, E. L. 1975 Stability of supercritical Bénard convection and Taylor vortex flow. *Adv. Chem. Phys.* **32**, 109–133.

LANDAU, L. 1944 On the problem of turbulence. *C.R. Acad. Sci. U.R.S.S.* **44**, 311–315.

LANDAU, L. & LIFSHITZ, E. M. 1959 *Fluid Mechanics*, pp. 103–107. Reading, Mass.: Academic Press.

LORENZ, E. N. 1963 Deterministic non-periodic flow. *J. Atm. Sci.* **20**, 130–141.

MALLOCK, A. 1888 Determination of the viscosity of water. *Proc. Roy. Soc.* A **45**, 126–132.

MALLOCK, A. 1896 Experiments on fluid viscosity. *Phil. Trans. Roy. Soc.* A **187**, 41–56.

MARSDEN, J. E. & MCCRACKEN, M. 1976 *The Hopf Bifurcation and its Applications*. Appl. Math. Sci. vol. 19. Springer.

MEYER, K. A. 1969 Three-dimensional study of flow between concentric rotating cylinders. In *High Speed Computing in Fluid Dynamics, Phys. Fluids Suppl.* II, 165–170.

NEWHOUSE, S., RUELLE, D. & TAKENS, F. 1978 Occurrence of strange Axiom A attractors near quasi-periodic flows on T^m, $m \geqslant 3$. *Commun. Math. Phys.* **64**, 35–40.

OTNES, R. K. & ENOCHSON, L. 1978 *Applied Time Series Analysis*. New York: Wiley.

RAYLEIGH, LORD 1920 On the dynamics of revolving fluids. *Scientific Papers*, vol. 6, 447–453. Cambridge University Press.

ROBERTS, P. H. 1965 Appendix in Experiments on the stability of viscous flow between rotating cylinders. VI. Finite-amplitude experiments. *Proc. Roy. Soc.* A **283**, 531–556.

RUELLE, D. & TAKENS, F. 1971 On the nature of turbulence. *Commun. Math. Phys.* **20**, 167–192.

SCHULTZ-GRUNOW, F. & HEIN, H. 1956 Beitrag zur Couetteströmung. *Z. Flugwiss.* **4**, 28–30.

SCHWARZ, K. W., SPRINGETT, B. E. & DONNELLY, R. J. 1964 Modes of instability in spiral flow between rotating cylinders. *J. Fluid Mech.* **20**, 281–289.

SERRIN, J. 1959 On the stability of viscous fluid motions. *Arch. Rat. Mech. Anal.* **3**, 1–13.

SHERMAN, J. & MCLAUGHLIN, J. B. 1978 Power spectra of nonlinearly coupled waves. *Commun. Math. Phys.* **58**, 9–17.

SNYDER, H. A. 1968*a* Stability of rotating Couette flow. I. Asymmetric waveforms. *Phys. Fluids* **11**, 728–734.

SNYDER, H. A. 1968*b* Stability of rotating Couette flow. II. Comparison with numerical results. *Phys. Fluids* **11**, 1599–1605.

SNYDER, H. A. 1969*a* Wavenumber selection at finite amplitude in rotating Couette flow. *J. Fluid Mech.* **35**, 273–298.

SNYDER, H. A. 1969*b* Change in waveform and mean flow associated with wavelength variations in rotating Couette flow. *J. Fluid Mech.* **35**, 337–352.

SNYDER, H. A. 1970 Waveforms in rotating Couette flow. *Int. J. Nonlinear Mech.* **5**, 659–685.

SNYDER, H. A. & LAMBERT, R. B. 1966 Harmonic generation in Taylor vortices between rotating cylinders. *J. Fluid Mech.* **26**, 545–562.

SWINNEY, H. L., FENSTERMACHER, P. R. & GOLLUB, J. P. 1977*a* Transition to turbulence in circular Couette flow. In *Symposium on Turbulent Shear Flows*, Univ. Pennsylvania, Univ. Park, vol 2, p. 17.1.

SWINNEY, H. L., FENSTERMACHER, P. R. & GOLLUB, J. P. 1977*b* Transition to turbulence in a fluid flow. *Synergetics: a Workshop* (ed. H. Haken), pp. 60–69. Berlin: Springer.

SWINNEY, H. L. & GOLLUB, J. P. 1978 Transition to turbulence. *Physics Today*, **31** (8), 41–49.

TAYLOR, G. I. 1923 Stability of a viscous liquid contained between two rotating cylinders. *Phil. Trans. Roy. Soc.* A **223**, 289–343.

TEMAN, R. 1976 *Turbulence and Navier–Stokes Equations*. Springer Lecture Notes in Mathematics no. 565.

WALDEN, R. W. & DONNELLY, R. J. 1979 Re-emergent order of chaotic circular Couette flow. *Phys. Rev. Lett.* **42**, 301–304.

WALOWIT, J., TSAO, S. & DIPRIMA, R. C. 1964 Stability of flow between arbitrarily spaced concentric cylindrical surfaces including the effect of a radial temperature gradient. *Trans. J. Appl. Mech.* **31**, 585–593.

YAHATA, H. 1978 Temporal development of the Taylor vortices in a rotating fluid. *Prog. Theor. Phys. Suppl.* **64**, 165–185.

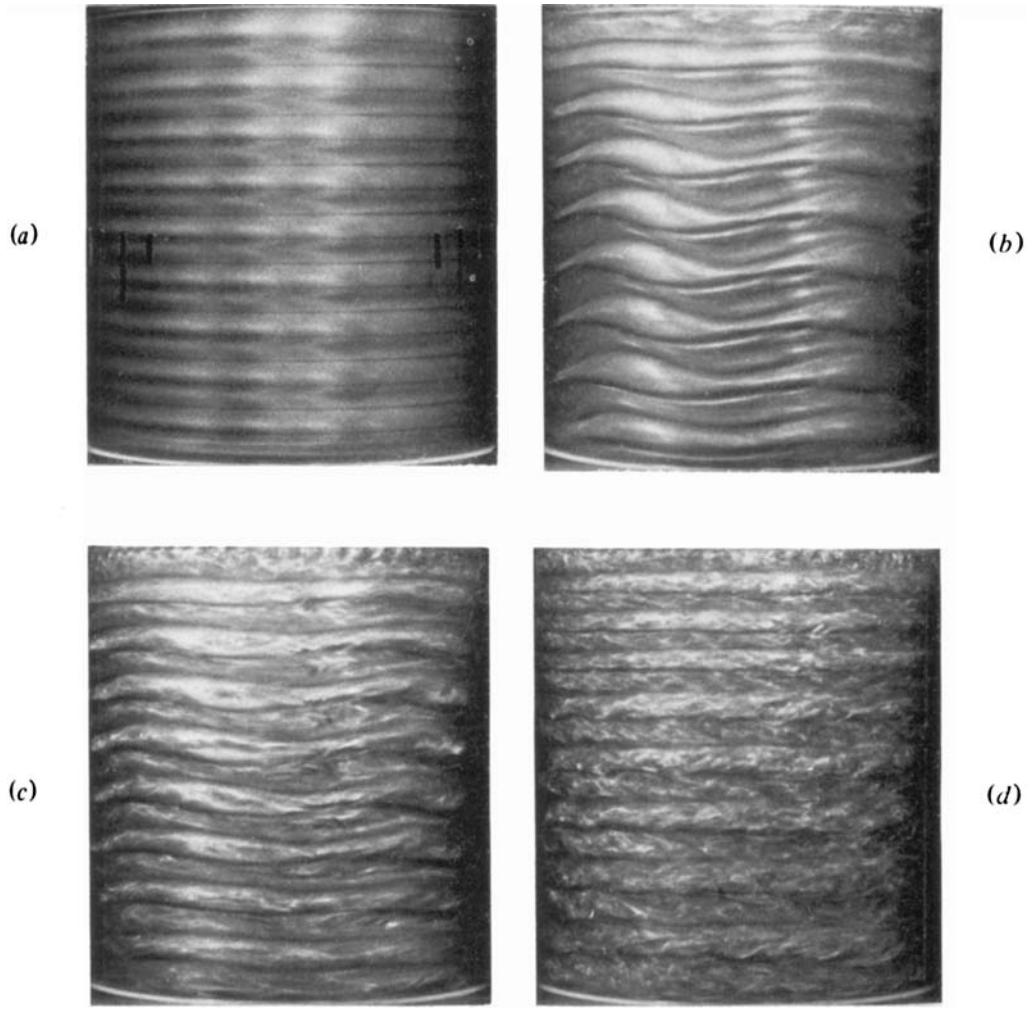

FIGURE 1. (*a*) $R/R_c = 1{\cdot}1$. Time-independent Taylor vortex flow with 18 vortices. The flows at the upper and lower fluid surfaces are inward. The vertical bars are fiducials separated by 10° angles. (*b*) $R/R_c = 6{\cdot}0$. (*c*) $R/R_c = 16{\cdot}0$. (*d*) $R/R_c = 23{\cdot}5$. Figures (*b*) and (c) illustrate wavy vortex flow (with 4 waves around the annulus), while in (*d*) the waves have disappeared. In (*b*), (*c*), and (*d*) there are 17 vortices, and the flow is outward at the upper surface and inward at the lower surface.

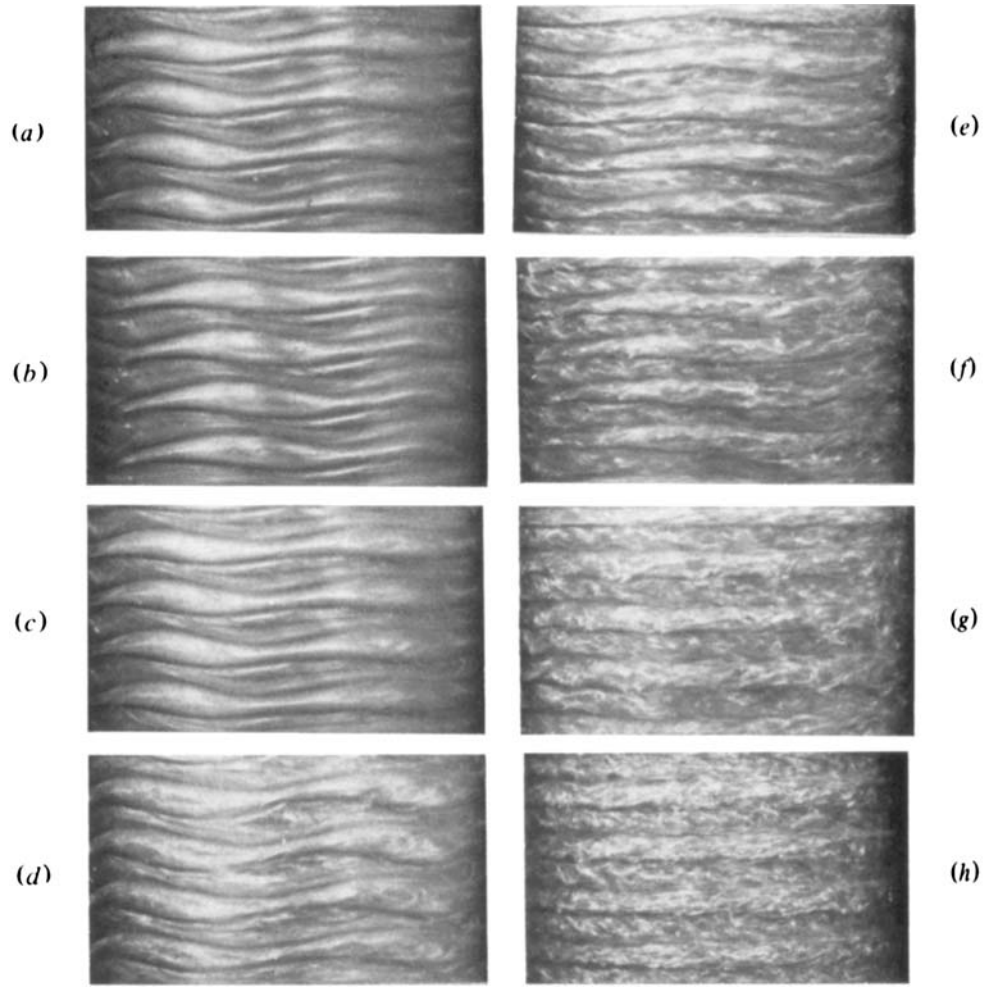

FIGURE 6. Photographs of the flow corresponding to the velocity graphs and power spectra in figure 5. The relative Reynolds numbers R/R_c are: (*a*) 9·5, (*b*) 10·5, (*c*) 11·0, (*d*) 15·0, (*e*) 19·0, (*f*) 21·5, (*g*) 23·0, (*h*) 43·3. There are 17 axial vortices and 4 azimuthal waves except in (*g*) and (*h*) where the waves have disappeared.